Microstructural modeling of early-age creep in hydrating cement paste

Do, Huy; Bishnoi, Shashank; Scrivener, Karen L.

DOI
10.1061/(ASCE)EM.1943-7889.0001144

Publication date
2016

Document Version
Accepted author manuscript

Published in
Journal of Engineering Mechanics

This is an Accepted Author Manuscript of an article published by ASCE in the Journal of Engineering Mechanics, available online: https://doi.org/10.1061/(ASCE)EM.1943-7889.0001144

Microstructural Modeling of Early-Age Creep in Hydrating Cement Paste

Quang Huy Do[1]; Shashank Bishnoi[2]; and Karen L. Scrivener[3]

Abstract: This paper presents a new approach to model the creep behavior of cement paste at early ages. The creep behavior is simulated by applying a time-varying generalized Maxwell model on the individual elements of a finite-element mesh of a simulated three-dimensional microstructure and compared with results in the literature. All mechanical properties of the constituent phases are taken from literature and Maxwell chain parameters are obtained by fitting the intrinsic creep of calcium silicate hydrate (C-S-H). A reasonable agreement between the simulations and the experimental results are obtained by assuming a constant C-S-H density of 2.0 g/cm^3. It was found that better agreements could be obtained at low degree of hydrations, by assuming a loosely packed C-S-H growing in the microstructure. It was also found that the short-term creep characteristics of C-S-H from nanoindentation can be used to reproduce macroscopic creep at least over a few days. The results show how numerical models can be used to upscale phase characteristics to macroscopic properties of composites.

Author keywords: Ageing creep; Finite-element method; Modeling; Cement microstructure; Calcium silicate hydrate (C-S-H); Calcium silicate hydrate (C-S-H) densification; Early-age properties; Microstructural modeling.

Introduction

Creep in hardening cement pastes significantly affects their stress development and time-dependent deformation. Creep is often modeled using viscoelastic constitutive equations and the detailed knowledge about the viscoelastic behavior at early ages is important in predicting the possibility of early-age cracking due to shrinkage and thermal stresses. Early-age creep is difficult to predict because the microstructure evolves after the application of the initial load and creeps nonuniformly. Despite its practical importance, there are very limited experimental data on the creep properties of cement paste at ages less than 72 h in literature. Experiments on creep during this period are very difficult to carry out and interpret due to the relatively soft but rapidly stiffening microstructure.

Models to predict the long-term creep of cement pastes are usually based on mathematical functions that fit empirical data (Bažant and Baweja 2000; Grasley and Lange 2007) or based on micromechanical models (Pichler and Lackner 2008; Scheiner and Hellmich 2009). Such models assume a random distribution of the phases in the microstructure, and while some models consider the geometry of phases, they do not take the spatial arrangement of the phases into account. In the other approach, computer-based numerical models can represent more realistic microstructural configurations and offer the possibility of tracking the evolution of detailed stress and strain states at the microstructural level (Šmilauer and Bažant 2010; Sanahuja and Toulemonde 2011; Sedef et al. 2006).

While it is generally agreed that creep of cement paste originates in calcium silicate hydrate (C-S-H) (Ulm et al. 1999; Velez et al. 2001; Bernard et al. 2003; Vandamme 2008), homogeneous C-S-H identical to the C-S-H in a hydrating cement paste seems impossible to prepare at scales suitable for mechanical testing. The identification of C-S-H properties therefore comes from one of two approaches:

1. Microstructural inverse analysis from creep data of cement paste or concrete. For example, the concrete creep model at the macrolevel developed by Bazant and Baweja (2000) was used to adapt to the C-S-H phase. The solidification theory by Bažant is based on the idea that the aging aspect is due to growth of the volume fraction of load-bearing portion of solidified matter whose properties are age independent.
2. Short-term nanoindentation measurements (Constantinides and Ulm 2007; Vandamme 2008; Vandamme and Ulm 2009) over some minutes at the scale of 0.1 μm, at which the C-S-H is assumed to be homogenous.

In this study, the latter is used because it is more suitable for modeling of creep behavior over a time span from a few hours to a few days.

A recent work (Do et al. 2015) in linear elastic homogenization for the cement paste microstructure demonstrated the potential of numerical homogenisation using finite-element (FE) analysis. In that study, so-called burning algorithms were developed to remove the artificial connections induced by the limited resolution of FE meshes. The calculated effective elastic properties of the microstructure using FE analysis were in good agreement with the experimental results.

This paper presents a new numerical approach for prediction the ageing creep in early-age cement paste. The simulations only need as input the mixture characteristics. The microstructure results from the hydration simulation and the mechanical simulations then use only the intrinsic properties of chemical phases. The creep behavior at the paste scale of the digital microstructures generated by μic (Bishnoi and Scrivener 2009) is obtained by means of numerical

[1]Researcher, Transport Engineering and Logistics Section, Delft Univ. of Technology, Room B3200, Building 34, Mekelweg 2, 2628 CD, Delft, Netherlands.

[2]Assistant Professor, Dept. of Civil Engineering, Indian Institute of Technology Delhi, Hauz Khas, New Delhi 110016, India (corresponding author). E-mail: shashank.bishnoi@gmail.com

[3]Professor, Ecole Polytechnique Fédérale de Lausanne, EPFL-STI-IMX-LMC, 1015 Lausanne, Switzerland.

homogenization using FE analysis using the burning algorithms discussed previously. The linear viscous properties of C-S-H from measured nanoindentation (Vandamme 2008) are numerically represented using generalized Maxwell chains. The creep compliances of the digital microstructures for different ages of loading are calculated under a sustained constant stress. The novelty in this study is that the creep simulations for very young ages of loading take into account the rapidly changing microstructure due to continuing hydration. In the early stage of hydration, when the microstructure still has a loose spatial structure, characterized by a sparse distribution of solids and a low packing C-S-H density, the solid skeleton tends to deform relatively easily. During the continuing hydration process, the new hydrates are progressively filling up in the spatial microstructure and, at the same time, previously formed C-S-H elements gradually are hardened by increasing their density, which stiffen the microstructure and restrain the viscous deformations. Once new hydrates have been formed, the relaxation of existing C-S-H results in the internal loads that are then redistributed on hydrates formed at different times. Therefore, this approach considers both the formation of new C-S-H and C-S-H densification.

For validation with experiment, the inputs of the simulations are based on the data set for a cement paste at water to cement ratio of 0.5 from Tamtsia et al. (2004) with which the outputs of the creep simulations at three different ages of loading are compared. Due to scarcity of experimental data for early-age creep of cement paste, only this data set has been found to be sufficient for validation of the simulations.

Homogenization Based on Finite-Element Method

The elastic and viscoelastic responses of chemical phases in the cement paste microstructures are considered. The continuum FE formulation for elasticity boundary value problems can be found in elsewhere (Turner et al. 1956; Argyris and Kelsey 1954; Zienkiewicz and Taylor 2000). Only the derivations here related to a viscoelastic material are described.

Formalized Governing Equations for Linear Viscoelastic Boundary Value Problems

In this paper, $\mathbf{u}$, $\boldsymbol{\sigma}$, and $\boldsymbol{\varepsilon}$ denote the displacement vector, the Cauchy stress tensor, and the infinitesimal strain tensor, respectively. The strong form of a boundary value problem for each infinitesimal point at time t within a given spatial domain Ω under the static condition can be formulated as

$$\text{Equilibrium: } \nabla^T \boldsymbol{\sigma}(t) + \mathbf{b}(t) = 0 \tag{1}$$

$$\text{Kinematics: } \boldsymbol{\varepsilon}(t) = \nabla \mathbf{u}(t) \tag{2}$$

Constitutive linear viscoelasticity:

$$\boldsymbol{\sigma}(t) = \int_0^t \mathbf{R}(t, t') : [d\boldsymbol{\varepsilon}(t') - d\boldsymbol{\varepsilon}^0(t')] \tag{3}$$

The boundary conditions prescribed on Γ read

The displacement (also called Dirichlet) boundary condition Γ_u:

$$\mathbf{u} = \hat{\mathbf{u}} \tag{4}$$

The traction force (also called Neumann) boundary condition Γ_t:

$$\mathbf{t} = \boldsymbol{\sigma}\mathbf{n} = \hat{\mathbf{t}} \tag{5}$$

where ∇ = gradient operator; $\mathbf{b}$ = body force vector; $\mathbf{R}$ = fourth-rank tensorial stress relaxation function; t' = time at which strain is imposed; $d\varepsilon^0(t')$ = shrinkage (and thermal expansion) increments; $\hat{\mathbf{u}}$ = prescribed displacement vector; $\mathbf{t}$ = traction force vector; $\hat{\mathbf{t}}$ = prescribed traction force vector; and $\mathbf{n}$ = unit normal vector. The boundary conditions must satisfy $(\Gamma = \Gamma_u \cup \Gamma_t) \Lambda (\Gamma_u \cap \Gamma_t = \emptyset)$.

The preceding boundary value problem must be numerically solved due to the complexity of the microstructural geometry. As seen from governing Eqs. (1)–(5), a viscoelastic boundary value problem differs from an elastic one in the constitutive Eq. (3) described by internal variables. This stress relaxation behavior leads to the appearance of internal viscous forces in the left-hand side of the FE balance equation as discussed in the following.

Numerical Approach

Constitutive Linear Viscoelasticity based on Internal Variables

The method of internal variables (Zienkiewicz et al. 1968; Huet 1993; Guidoum 1994) is used here to eliminate the dependency of the entire response history. Hence the response at a given discrete time requires only the stress-strain states and the internal variables from the previous time step, which are induced by the applied load history.

According to thermodynamics, the canonical system of governing equations describing the rheological behavior of viscoelasticity for any infinitesimal material point is

$$\frac{\partial \mathfrak{R}}{\partial \dot{\boldsymbol{\varepsilon}}} + \frac{\partial \Phi}{\partial \boldsymbol{\varepsilon}} = \boldsymbol{\sigma} \tag{6}$$

$$\frac{\partial \mathfrak{R}}{\partial \dot{\beta}} + \frac{\partial \Phi}{\partial \beta} = \mathbf{0} \tag{7}$$

where Φ = potential free energy function; $\mathfrak{R}$ = Rayleigh kinetic potential dissipation function; and β = thermodynamic state variables tensor or internal variable tensor.

The stress and strain tensors of isotropic materials in the multiaxial case can be decomposed into volumetric and deviatoric parts

$$\sigma_{ij} = \sigma_m \delta_{ij} + \sigma_{ij}^d \tag{8}$$

$$\varepsilon_{ij} = \varepsilon_m \delta_{ij} + \varepsilon_{ij}^d \tag{9}$$

$$\beta_{ij} = \beta_m \delta_{ij} + \beta_{ij}^d \tag{10}$$

where δ_{ij} = Kronecker delta representing the identity matrix.

To describe the constitutive laws of linear viscoelastic materials in detail, it is necessary to define explicitly the two functions Φ and $\mathfrak{R}$. A generalized Maxwell model shown in Fig. 1 is used to describe numerically the material response. This model is a combination of several Maxwell elements that are assembled in parallel. It takes into account the material relaxation that does not occur at a single time, but over several time intervals: it functions as a piecewise linear approximation of the relaxation function in time. Fig. 1 illustrates the relaxation of the bulk modulus K and shear modulus G in the case of triaxial stress-strain relation. Individual segments correspond to different time periods, with shorter ones contributing less than longer ones, which allows the modeling of both short- and long-term viscoelastic responses given a large enough number of segments.

The potential free energy function Φ and the potential dissipation function $\mathfrak{R}$ in the generalized Maxwell isotropic material with the internal variables are expressed as

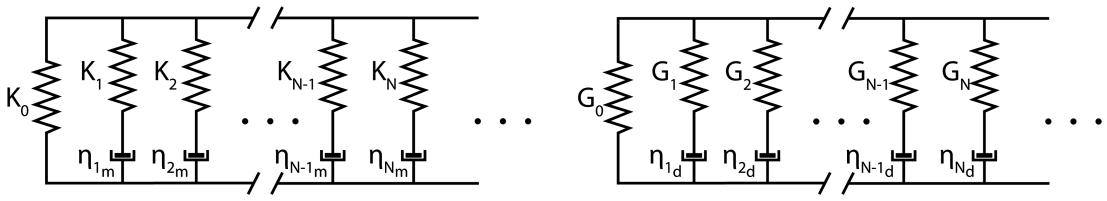

Fig. 1. Generalized Maxwell model constituted by spring-dashpot Maxwell elements assembled in parallel: (a) bulk modulus; (b) shear modulus

$$\Phi = \frac{1}{2}\left[K_0(3\varepsilon_m)^2 + \sum_{\alpha=1}^{N} K_\alpha(3\varepsilon_m - 3\beta_{\alpha_m})^2\right] + G_0\varepsilon_{ij}^d\varepsilon_{ij}^d + \sum_{\sigma=1}^{N} G_\alpha(\varepsilon_{ij}^d - \beta_{\alpha_{ij}}^d)(\varepsilon_{ij}^d - \beta_{\alpha_{ij}}^d) \tag{11}$$

$$\mathfrak{R} = \frac{1}{2}\sum_{\alpha=1}^{N} \eta_{\alpha_m}(3\beta_{\alpha_m})^2 + \sum_{\alpha=1}^{N} \eta_{\alpha_d}\dot{\beta}_{\alpha_{ij}}^d\dot{\beta}_{\alpha_{ij}}^d \tag{12}$$

where β_{α_m} and $\beta_{a_{ij}}^d$ are internal volumetric strain scalar and internal deviatoric strain tensors, respectively, of the damper in branch α. They are called the internal variables because they cannot be measured macroscopically. Variables η_{α_m} and η_{α_d} = viscosity of the material.

Substitution of functions Φ and $\mathfrak{R}$ of Eqs. (11) and (12) into Eq. (6) leads to the force equilibrium equation for all the branches

$$\sigma_{ij} = 3\left[K_0\varepsilon_m + \sum_{\alpha=1}^{N} K_\alpha(\varepsilon_m - \beta_{\alpha_m})\right]\delta_{ij} + 2\left[G_0\varepsilon_{ij}^d + \sum_{\sigma=1}^{N} G_\alpha(\varepsilon_{ij}^d - \beta_{\alpha_{ij}}^d)\right] \tag{13}$$

Substitution of functions Φ and $\mathfrak{R}$ of Eqs. (11) and (12) into Eq. (7) leads to the force equilibrium equations of volumetric deviatoric parts for each branch

$$3\eta_{\alpha_m}\dot{\beta}_{\alpha_m} - 3K_\alpha(\varepsilon_m - \beta_{\alpha_m}) = 0 \quad \alpha = 1, N \tag{14}$$

$$2\eta_{\alpha_d}\dot{\beta}_{\alpha_{ij}}^d - 2G_\alpha(\varepsilon_{ij}^d - \beta_{\alpha_{ij}}^d) = 0 \quad \alpha = 1, N \tag{15}$$

The constitutive law is defined if all the internal variables β_{α_m} and $\beta_{\alpha_{ij}}^d$ are known. The solution can be obtained by integrating the differential equations system of Eqs. (14) and (15)

With the definition of the relaxation time

$$\tau_\alpha = \frac{\eta_{\alpha_m}}{K_\alpha} = \frac{\eta_{\alpha_d}}{G_\alpha} \tag{16}$$

Eq. (14) becomes

$$\dot{\beta}_{\alpha_m} + \frac{1}{\tau_\alpha}\beta_{\alpha_m} = \frac{1}{\tau_\alpha}\varepsilon_m \quad \alpha = 1, N \tag{17}$$

and Eq. (15) becomes

$$\dot{\beta}_{\alpha_{ij}}^d + \frac{1}{\tau_\alpha}\beta_{\alpha_{ij}}^d = \frac{1}{\tau_\alpha}\varepsilon_{\alpha_{ij}}^d \quad \alpha = 1, N \tag{18}$$

The analytical solution of system Eq. (14) is written in a convolution integral

$$\beta_{\alpha_m} = \int_0^t \left[1 - e^{-(t-\tau/\tau_\alpha)}\right]\dot{\varepsilon}_m(\tau)d\tau \quad \alpha = 1, N \tag{19}$$

The analytical solution of system Eq. (15) is written in a convolution integral

$$\beta_{\alpha_{ij}}^d = \int_0^t \left[1 - e^{-(t-\tau/\tau_\alpha)}\right]\dot{\varepsilon}_{ij}^d(\tau)d\tau \quad \alpha = 1, N \tag{20}$$

For the FE analysis, these equations require integration over finite time intervals. In this numerical approach, the strain rate $\dot{\varepsilon}_m$ and $\dot{\varepsilon}_{ij}^d$ are assumed to be constant within each time interval Δt_h, but change at steps t_h. This assumption gives the solution for the internal variables β_{α_m} and $\beta_{\alpha_{ij}}^d$ at the time t_h, and they are expressed recursively as

$$\beta_{\alpha_{m_h}} = e^{-(\Delta t_h/\tau_\alpha)}\beta_{\alpha_{m_{h-1}}} + \Delta\varepsilon_{m_h}\left\{1 - \frac{\tau_\alpha}{\Delta t_h}\left[1 - e^{-(\Delta t_h/\tau_\alpha)}\right]\right\} + \varepsilon_{m_{h-1}}\left[1 - e^{-(\Delta t/\tau_\alpha)}\right] \tag{21}$$

$$\beta_{\alpha_{ij_h}}^d = e^{-(\Delta t_h/\tau_\alpha)}\beta_{\alpha_{ij_{h-1}}}^d + \Delta\varepsilon_{ij_h}^d\left\{1 - \frac{\tau_\alpha}{\Delta t_h}\left[1 - e^{-(\Delta t_h/\tau_\alpha)}\right]\right\} + \varepsilon_{ij_{h-1}}^d\left[1 - e^{-^{-(\Delta t/\tau_\alpha)}}\right] \tag{22}$$

where

$$\Delta t_h = t_h - t_{h-1} \quad \text{and} \quad \Delta\varepsilon_{m_h} = \varepsilon_{m_h} - \varepsilon_{m_{h-1}} \quad \text{and} \quad \Delta\varepsilon_{ij_h}^d = \varepsilon_{ij_h}^d - \varepsilon_{ij_{h-1}}^d \tag{23}$$

Once the increment of internal variables are defined as

$$\Delta\beta_{\alpha_{m_h}} = \beta_{\alpha_{m_h}} - \beta_{\alpha_{m_{h-1}}} \tag{24}$$

and

$$\Delta\beta_{\alpha_{ij_h}}^d = \beta_{\alpha_{ij_h}}^d - \beta_{\alpha_{ij_{h-1}}}^d \tag{25}$$

The solutions then can be rewritten

$$\Delta\beta_{\alpha_{m_h}} = [1 - e^{-(\Delta t/\tau_\alpha)}](\varepsilon_{m_{h-1}} - \beta_{\alpha_{m_{h-1}}}) + (1 - \lambda_\alpha)\Delta\varepsilon_{m_h} \tag{26}$$

$$\Delta\beta_{\alpha_{ij_h}}^d = [1 - e^{-(\Delta t/\tau_\alpha)}](\varepsilon_{ij_{h-1}}^d - \beta_{\alpha_{ij_{h-1}}}^d) + (1 - \lambda_\alpha)\Delta\varepsilon_{ij_h}^d \tag{27}$$

where

$$\lambda_\alpha = [1 - e^{-(\Delta t/\tau_\alpha)}]\frac{\tau_\alpha}{\Delta t} \tag{28}$$

The increment of the total stress in Eq. (13) can also be written in an incremental form at time t_h

$$\Delta\sigma_{ij_h} = 3\left[K_0\Delta\varepsilon_{m_h} + \sum_{\alpha=1}^{N} K_\alpha(\Delta\varepsilon_{m_h} - \Delta\beta_{\alpha_{m_h}})\right]\delta_{ij} + 2\left[G_0\Delta\varepsilon^d_{ij_h} + \sum_{\sigma=1}^{N} G_\alpha(\Delta\varepsilon^d_{ij_h} - \Delta\beta^d_{\alpha_{ij_h}})\right] \tag{29}$$

Thus the equation in short

$$\Delta\sigma_{ij_h} = \Delta\sigma_{m_h}\delta_{ij} + \Delta\sigma^d_{ij_h} \tag{30}$$

where

$$\Delta\sigma_{m_h} = 3\left[K_0\Delta\varepsilon_{m_h} + \sum_{\alpha=1}^{N} K_\alpha(\Delta\varepsilon_{m_h} - \Delta\beta_{\alpha_{m_h}})\right] \tag{31}$$

and

$$\sigma^d_{ij_h} = 2\left[G_0\Delta\varepsilon^d_{ij_h} + \sum_{\sigma=1}^{N} G_\alpha(\Delta\varepsilon^d_{ij_h} - \Delta\beta^d_{\alpha_{ij_h}})\right] \tag{32}$$

With the substitution of $\Delta\beta_{\sigma_{m_h}}$ of Eq. (26) into Eq. (31), an explicit relation between volumetric stress and volumetric strain in an incremental form can be rewritten as

$$\Delta\sigma_{m_h} = 3\left(K_0 + \sum_{\alpha=1}^{N} K_\alpha\cdot\lambda_\alpha\right)\Delta\varepsilon_{m_h} - 3\sum_{\alpha=1}^{N} K_\alpha[1 - e^{-(\Delta t/\tau_\alpha)}](\varepsilon_{m_{h-1}} - \beta_{\alpha_{m_{h-1}}}) \tag{33}$$

Similarly with the substitution of $\Delta\beta^d_{\sigma_{ij_h}}$ of Eq. (27) into Eq. (32), an explicit relation between deviatoric stress and deviatoric strain in an incremental form can be rewritten as

$$\Delta\sigma^d_{ij_h} = 2\left(G_0 + \sum_{\alpha=1}^{N} G_\alpha\cdot\lambda_\alpha\right)\Delta\varepsilon^d_{ij_h} - 3\sum_{\alpha=1}^{N} G_\alpha[1 - e^{-(\Delta t/\tau_\alpha)}](\varepsilon^d_{ij_{h-1}} - \beta^d_{\alpha_{ij_{h-1}}}) \tag{34}$$

Eq. (33) can be rewritten in short

$$\Delta\sigma_{m_h} = 3(\bar{K}\Delta\varepsilon_{m_h} + \Delta\overline{\sigma_{m_h}}), \quad \text{thus } \Delta\sigma_m = 3(\bar{K}\Delta\varepsilon_m + \Delta\overline{\sigma_m}) \tag{35}$$

where

$$\bar{K} = K_0 + \sum_{\alpha=1}^{N} K_\alpha\cdot\lambda_\alpha \tag{36}$$

and

$$\Delta\overline{\sigma_{m_h}} = -\sum_{\alpha=1}^{N} K_\alpha[1 - e^{-(\Delta t/\tau_\alpha)}](\varepsilon_{m_{h-1}} - \beta_{\alpha_{m_{h-1}}}) \tag{37}$$

Eq. (34) can be rewritten in short

$$\Delta\sigma^d_{ij_h} = 2(\bar{G}\Delta\varepsilon^d_{ij_h} + \Delta\overline{\sigma^d_{ij_h}}), \quad \text{thus } \Delta\sigma^d_{ij} = 2(\bar{G}\Delta\varepsilon^d_{ij} + \Delta\overline{\sigma^d_{ij}}) \tag{38}$$

where

$$\bar{G} = G_0 + \sum_{\alpha=1}^{N} G_\alpha\cdot\lambda_\alpha \tag{39}$$

and

$$\Delta\overline{\sigma^d_{ij_h}} = -\sum_{\alpha=1}^{N} G_\alpha[1 - e^{-(\Delta t/\tau_\alpha)}](\varepsilon^d_{ij_{h-1}} - \beta^d_{\alpha_{ij_{h-1}}}) \tag{40}$$

By recalling Eq. (8), the decomposition of the stress tensor in an increment form reads

$$\Delta\sigma_{ij} = \Delta\sigma_m\delta_{ij} + \Delta\sigma^d_{ij} \tag{41}$$

Substituting Eqs. (35) and (38) into Eq. (41) leads to the relation between the stress and strain tensors

$$\Delta\sigma_{ij} = 3\bar{K}\Delta\varepsilon_m\delta_{ij} + 2\bar{G}\Delta\varepsilon^d_{ij} + 3\Delta\bar{\sigma}_m\delta_{ij} + 2\Delta\overline{\sigma^d_{ij}} \tag{42}$$

This relation can be rewritten in a matrix notation for the FE implementation

$$\Delta\boldsymbol{\sigma} = \bar{\mathbf{D}}{:}\Delta\boldsymbol{\varepsilon} + \Delta\bar{\boldsymbol{\sigma}} \tag{43}$$

where

$$\Delta\overline{\sigma_{ij}} = 3\Delta\bar{\sigma}_m\delta_{ij} + 2\Delta\overline{\sigma^d_{ij}} \tag{44}$$

and $\bar{\mathbf{D}}$ is a fourth-rank tensor that can be represented by a 6×6 matrix as

$$\bar{\mathbf{D}} = \begin{bmatrix} \bar{K}+4\bar{G}/3 & \bar{K}-2\bar{G}/3 & \bar{K}-2\bar{G}/3 & 0 & 0 & 0 \\ & \bar{K}+4\bar{G}/3 & \bar{K}-2\bar{G}/3 & 0 & 0 & 0 \\ & & \bar{K}+4\bar{G}/3 & 0 & 0 & 0 \\ & & & \bar{G} & 0 & 0 \\ & Sym & & & \bar{G} & 0 \\ & & & & & \bar{G} \end{bmatrix} \tag{45}$$

Finite-Element Formulation

Derived from the equilibrium Eq. (1), the FE equilibrium in the incremental form to relate internal and external forces of an element in the domain Ω for a viscoelastic material reads

$$\int_{\Omega^e} \mathbf{B}^T\Delta\boldsymbol{\sigma}d\Omega = \Delta\mathbf{F}^e_{ex} \tag{46}$$

where $\Delta\mathbf{F}^e_{ex}$ = external node vector; and $\mathbf{B}$ = strain displacement matrix.

The strain displacement matrix $\mathbf{B}$ maps the element displacement vector $\mathbf{d}$ onto the strain vector $\boldsymbol{\varepsilon}$. The incremental form of this relation reads

$$\Delta\boldsymbol{\varepsilon} = \mathbf{B}\Delta\mathbf{d} \tag{47}$$

Substitution of Eq. (43) into Eq. (46) leads to

$$\int_{\Omega^e} \mathbf{B}^T(\bar{\mathbf{D}}\,\Delta\boldsymbol{\varepsilon} + \Delta\bar{\boldsymbol{\sigma}})d\Omega = \Delta\mathbf{F}^e_{ex} \tag{48}$$

Substitution of Eq. (47) into Eq. (48) reads

$$\int_{\Omega^e} \mathbf{B}^T(\bar{\mathbf{D}}\mathbf{B}\Delta\mathbf{d} + \Delta\bar{\boldsymbol{\sigma}})d\Omega = \Delta\mathbf{F}^e_{ex} \tag{49}$$

Rearrangement of Eq. (49) reads

$$\int_{\Omega^e} (\mathbf{B}^T\bar{\mathbf{D}}\mathbf{B})d\Omega\Delta\mathbf{d} = \Delta\mathbf{F}^e_{ex} - \int_{\Omega^e} \mathbf{B}^T\Delta\bar{\boldsymbol{\sigma}}d\Omega \tag{50}$$

The element stiffness matrix is defined as

$$\mathbf{K}^e = \int_{\Omega^e} (\mathbf{B}^T\bar{\mathbf{D}}\mathbf{B})d\Omega \tag{51}$$

By substituting Eq. (51) into Eq. (50), the canonical format for a FE procedure reads

$$\mathbf{K}^e\Delta\mathbf{d} = \Delta\mathbf{F}^e_{ex} - \int_{\Omega^e} \mathbf{B}^T\Delta\bar{\boldsymbol{\sigma}}d\Omega \tag{52}$$

The global balance equations for the entire system corresponding to the boundary value problem are obtained by assembling Eq. (52) for all elements in the domain Ω. In Eq. (52), the right-hand-side terms are known. Therefore, at each time step, the FE procedure solves for the incremental displacement at every node and incremental stress and strain at every integration point.

In the creep simulations in this study, a constant load with time is applied and the load increment $\Delta\mathbf{F}^e_{ex}$ is set to zero tensor: $\Delta\mathbf{F}^e_{ex} \equiv \mathbf{0}$. For spatial discretization, regular cubic elements with trilinear shape functions are used.

Intrinsic Short-Term C-S-H Creep Function

Experimental Data

The intrinsic creep properties of C-S-H are adopted from the experimental results of Vandamme and Ulm (2009) and Vandamme (2008). In their work, the in situ creep behavior of C-S-H, the nanocrystalline phase which forms the major part of hydrated cement paste was measured by means of a statistics on nanoindentation results. There is some debate as to the specificity of nanoindentation measurement because the volume sampled is in fact of the order of some micrometers in dimension and may contain other phases finely intermixed with C-S-H. However, this spatial resolution is of the same order as the mesh size used in present finite-element method (FEM) simulations so the data are considered appropriate despite these reservations.

According to Vandamme (2008), the creep compliance of any type of C-S-H can be presented as a logarithmic form

$$L(t, t_0) = \frac{1}{M} + \frac{1}{C}\ln\left(1 + \frac{t - t_0}{\tau}\right) \tag{53}$$

where $L(t, t_0)$ (GPa^{-1}) = contact creep compliance at a certain time t of the material loaded from time t_0 (h); M (GPa) = elastic indentation module; C (GPa) = contact creep module; and τ (s) = characteristic viscous time.

From the experimental results and the extrapolation based on self-constant scheme, Vandamme (2008) obtained the correlation between the contact creep modulus C and the packing density η of C-S-H as

$$C = 1{,}588.9(\eta - 0.5)^{1.597} \tag{54}$$

Eq. (54) implies that the upscaling method using the self-consistent theory with the spherical granular morphology of the C-S-H particles on their packing density is characterized by a percolation threshold of 0.5 of solid fraction, below which the composite C-S-H has no stiffness. The percolation threshold strongly depends on the homogenization scheme and the assumptions of morphology of the composite material (Vandamme 2008).

Similar to the contact creep compliance in Eq. (53), the uniaxial creep compliance can be described as follows:

$$J(t, t_0) = \frac{1}{E} + \frac{1}{C_{\text{uni}}}\ln\left(1 + \frac{t - t_0}{\tau}\right) \tag{55}$$

where $J(t, t_0)$ (GPa^{-1}) = uniaxial creep compliance a certain time t of the material loaded from time t_0; E (GPa) = elastic module of C-S-H; and C_{uni} (GPa) = uniaxial creep modulus.

The relations between the contact and uniaxial parameters in Eqs. (53) and (55) are

$$\frac{E}{M} = \frac{C_{\text{uni}}}{C} = 1 - \nu^2 \tag{56}$$

where ν (—) = Poisson's ratio of C-S-H.

In this study, simulations are carried out assuming two cases of C-S-H density: a constant density $\rho = 2.0$ g/cm^3 and densification. A traction load is applied on the boundary of the microstructure from time t_0 and kept constant throughout creep simulations.

Generalized Maxwell Model Derived from Nanoindentation Data for C-S-H Constant Density $\rho = 2.0$ g/cm^3

To determine the creep function of C-S-H from the experimental data, all parameters, i.e., E, C_{uni}, and τ, of Eq. (55) must be known. C-S-H bulk density 2.0 g/cm^3 is the typical value reported in the literature (Thomas and Jennings 2006). The creep simulations for cement paste are performed using only one creep function of C-S-H that corresponds to its constant bulk density $\rho = 2.0$ g/cm^3, its packing density $\eta = 0.7$, initial Young's modulus $E = 25.55$ GPa, and constant Poisson's ratio $\nu = 0.24$. These parameters are then used to determine C_{uni} using Eqs. (54) and (56).

In Eq. (55), one unknown parameter is the characteristic viscous time τ. This coefficient was experimentally observed to have a weak correlation with the elastic indentation module M (Vandamme 2008). The mean value $\tau = 1.66$ s from the experiments of Vandamme (2008) is used in this study. Therefore, the intrinsic uniaxial creep function of C-S-H based on the nanoindentation experiments is fit by the solid line in Fig. 2. The coefficient of determination of the fit experimental data is $R^2 = 0.89$, for which the correlation between C and η in Eq. (54) mainly accounts. This fit creep function is not a linear function of time; however, in the logarithmic time scale in Fig. 2, C-S-H creep appears as linear.

Creep deformations of a cement paste could be distinguished generally into two domains: a short-term volumetric creep and a long-term deviatoric creep. The triaxial creep experiment on a leached cement paste (Bernard et al. 2003) revealed that the Lagrangian porosity decreases during approximately the first 21 days of loading and there is no significant change of porosity afterward. In this numerical model, however, it is reasonable to assume that the creep Poisson's ratio is approximately constant (Wendner et al. 2015), which implies coupling between the volumetric and deviatoric creep mechanisms. This pragmatic assumption may be made due to the fact that both simulated and experimental creeps in the present study are carried out under the uniaxial compression condition for some days after loading. Furthermore, these notions are

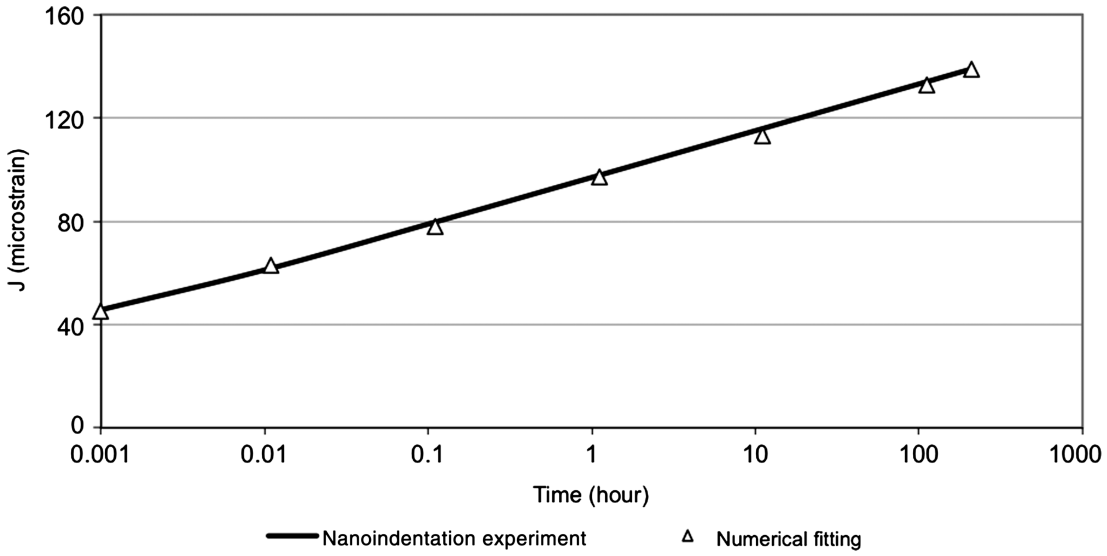

Fig. 2. Input uniaxial creep function $[J(t-t_0,t_0)]$ of C-S-H derived from Vandamme (2008)

to characterize the creep behavior in terms of a uniaxial creep compliance, whose generalization to a multiaxial constitutive law is straightforward.

To numerically input the C-S-H behavior into the FE model described in Section "Homogenisation based on Finite Element Method," the numerical algorithm of Bažant (1972) was used to predict the relaxation response from the fit creep function (i.e., the solid line in Fig. 2). Numerical parameters (i.e., series of K and G) of a generalized Maxwell model are used to calibrate the predicted relaxation curves. The generalized Maxwell chain parameters are listed in Table 1. The creep response of a structure made of only one viscoelastic finite element using these modeling parameters is shown by the open triangles in Fig. 2. It can be seen that the errors for transformation of a model creep function into Maxwell chain parameters are negligible.

Multigeneralized Maxwell Model for C-S-H Densification Creep Functions

It has been reported that the packing density of C-S-H is low at a lower degree of hydration and increases with the hydration process (Bishnoi and Scrivener 2009; Thomas et al. 2009; Muller et al. 2013a, b). To study this effect on creep properties of cement paste, the simulations of the hydrating microstructure and the inputs of intrinsic compliance of C-S-H are considered with the densification of C-S-H. The development of C-S-H bulk density ρ is assumed to increase with time using the function described in Do et al. (2013)

$$\rho(t)=\rho_0\left[1.0-\left(\frac{e^{-0.207t}+e^{-0.054t}}{2}\right)\right] \tag{57}$$

Table 1. Maxwell Chain Parameters

Branch index α	Bulk modulus K_α (MPa)	Shear modulus G_α (MPa)	Relaxation time τ_α (h)
5	4,890	3,076	0.001
4	3,556	2,237	0.01
3	2,419	1,521	0.7
2	978	615	40
1	978	615	700
0	3,556	2,237	$+\infty$

In Eq. (57), $\rho(t)$ is the density as a function of time, and ρ_0 is the maximum density, which is assumed to be 2.0 g/cm^3. If C-S-H is considered as a mixture of the C-S-H nanocrystalline regions (pure C-S-H with 0% gel porosity) and gel pores, the packing density η of C-S-H will have a linear relation with the bulk C-S-H density. Consequently, all the mechanical properties of C-S-H vary as a function of time. Fig. 3 shows the evolutions of the packing density [based on Eq. (57)] and contact creep modulus [calculated from Eq. (54)] of C-S-H.

The uniaxial creep functions of C-S-H are determined using Eq. (55), but the major difference between this function and the one used in the case without densification is that the C-S-H densification plays a role in reduction of the viscous component. A scheme to estimate C-S-H creep functions $J(t,t_i)$ for the microstructure loaded from time t_0 and C-S-H batches formed at different times t_i taking into account their densification is sketched in Fig. 4. These times are the computation time steps of the creep simulation. For the sake of illustrative simplification, in this figure a C-S-H particle is assumed to grow with both size and densification. At the start of each time interval, a new C-S-H layer is deposited on the surface of this particle formed in the previous time steps. Although this particle is assumed to be homogenous during hydration, its layers formed at different times have different load histories. Consequently, each layer is assumed to have its own viscoelastic response characterized by different creep functions. For loading from t_o, Fig. 4 illustrates creep functions $J(t,t_0)$, $J(t,t_1)$, $J(t,t_2)$, and $J(t,t_3)$ corresponding to the creep responses of the layers L_0, L_1, L_2, and L_3 of the C-S-H.

Function $J(t,t_0)$ for Layer L_0 Formed at Loading Time t_o

The creep function $J(t,t_0)$ (shown as the solid lines in Fig. 4) consists of one instantaneous part (the elastic deformation at loading t_0) and segments of the viscous parts that are described by creep functions corresponding to the ageing of C-S-H. For the first viscous segment, the viscous deformation rate of $J(t,t_0)$ within the time interval $[t_0,t_1]$ is derived from Eq. (55) with the C-S-H density at the time t_0. In a similar way for the second viscous segment, the rate of $J(t,t_0)$ within the time interval $[t_1,t_2]$ is derived from Eq. (55) with the C-S-H density at time t_1. Similarly, for the third and fourth segments of $J(t,t_0)$ within the time intervals $[t_2,t_3]$ and $[t_3,t_4]$ are derived with densities at the time t_2 and t_3, respectively.

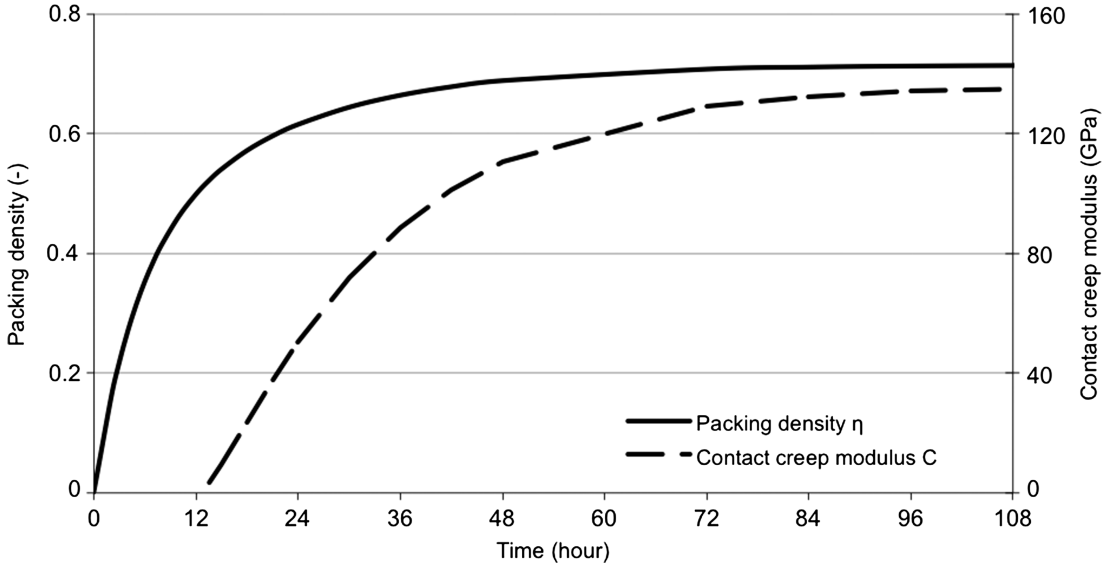

Fig. 3. Developments of packing density and contact creep modulus of C-S-H

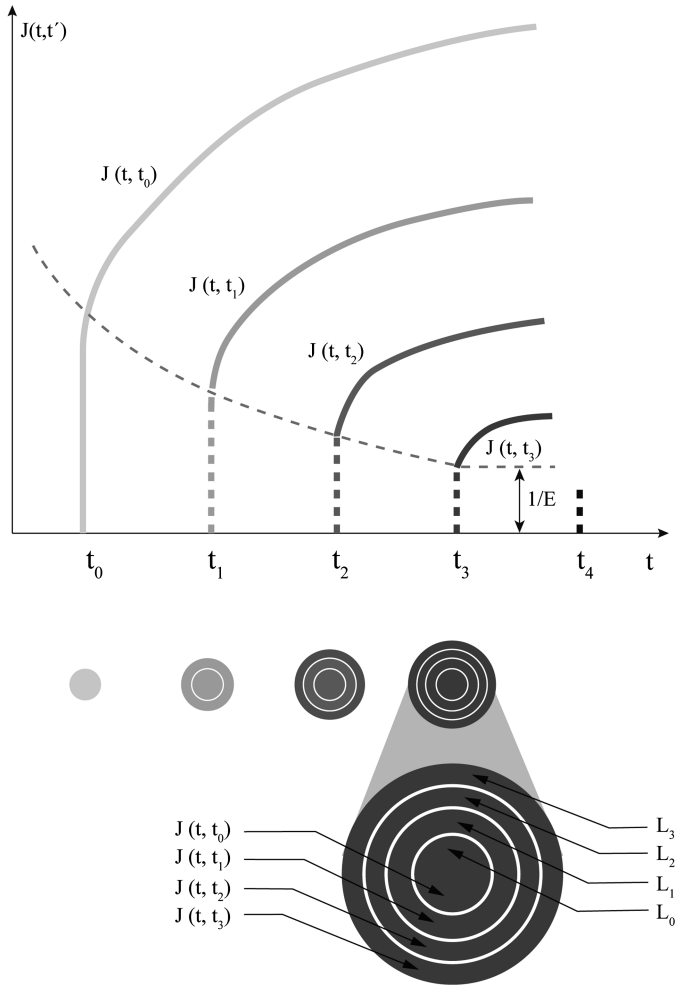

Fig. 4. Scheme to estimate C-S-H creep functions $J(t, t_i)$ for the creep simulation of cement paste for loading from t_0 taking into account densification; although this C-S-H particle is assumed to be homogenous during hydration, its layers formed at different times have different load histories; consequently, each layer is assumed to have its own viscoelastic response characterized by different creep functions

Due to densification, the slope of $J(t, t_0)$ decreases with time steps.

$J(t, t_0)$ is represented as

$$J_o(t, t_0) = \frac{1}{E(t_0)} + \frac{1}{C_{\text{uni}}(t)} \ln\left(1 + \frac{t - t_0}{\tau}\right) \quad \forall\ t \geq t_0 \tag{58}$$

Function $J(t,t_i)$ for Layer L_i Formed at Time $t_{i>0}$ after Loading Time t_o

The creep functions $J(t, t_i)$ with $I > 0$ (shown as the solid lines in Fig. 4) consist of segments of the viscous deformation, which are also derived from Eq. (55) corresponding to the C-S-H densities at $t_i, t_{i+1}, t_{i+2}, \ldots, t_{i+n}$. The rates of viscous deformation of $J(t, t_i)$ decreases with time steps.

$J(t, t_i)$ is represented as

$$J(t, t_i) = \frac{1}{C_{\text{uni}}(t)} \ln\left(1 + \frac{t - t_i}{\tau}\right) \quad \forall\ t \geq t_i > t_0 \quad \text{and} \quad \forall i > 0 \tag{59}$$

The solidification process during numerical creep testing is simulated by taking into account two factors: the formation of hydrates and C-S-H densification. With this densification, the C-S-H phases are heterogeneous in terms of the creep rate, but they are homogeneous in terms of density. For a creep simulation of cement paste for loading from t_0, apart from $J(t, t_0)$, all the densifying C-S-H phases characterized by creep functions $J(t, t_1)$, $J(t, t_2), J(t, t_3), \ldots, J(t, t_n)$ also play roles. To account for this fact, several generalized Maxwell models are used in the simulation for a given initial age of loading. In this multigeneralized Maxwell model, each material model is to fit a C-S-H creep function corresponding to the time at which those new C-S-H elements were formed, and an index array is used in the simulation program to keep track of the age of all C-S-H elements. In the FE procedure to simulate creep of cement paste for loading from t_0, only $J(t, t_0)$ is assumed to affect for both the elastic and viscous parts, whereas $J(t, t_1), J(t, t_2), J(t, t_3), \ldots, J(t, t_n)$ are considered to affect only the viscous part.

Materials and Hydration Simulation

Three-dimensional digital microstructures of cement paste are generated using the hydration model ***μic*** (Bishnoi and Scrivener 2009). Model ***μic*** is a modeling platform using the vector approach to simulate hydration of spherical particles in cement systems. By using many efficient algorithms, ***μic*** allows users to model a system having a particle size distribution similar to that of commercial cement. Model ***μic*** also offers users flexible mechanisms to define intrinsic kinetics, and distribution of products.

The hydration of a normal portland cement at a water-to-cement ratio of 0.5 is simulated. The input of cement mixture for the simulations is based on the experimental data from Tamtsia et al. (2004) with which the computed creep results will be compared. Based on the composition of the main minerals with the assumption of 5% gypsum content, the Bogue cement composition is C_3S (55%), C_2S (20%), C_3A (10.5%), and C_4AF (9.5%). The particle size distribution is obtained by fitting a Rosin-Rammler distribution (Taylor 1997) corresponding to a Blaine fineness of 3,400 cm^2/g. Hydration and creep properties are simulated on a cubic representative computational volume (CV) 100 μm in size (Do et al. 2013, 2015). The cement particles in the range from 0.1 to 40 μm in size are generated for the initial simulated microstructure.

The hydration degrees in the simulations are calibrated to match the profiles of hydration degree (at a constant relative humidity of $96 \pm 2\%$ and a constant temperature of 22 ± 2°C) as obtained by Tamtsia et al. (2004) from thermogravimetric analysis characterizing the state of water in the samples. Tamtsia et al. (2004) claimed that a sustained load for loading from 18 h applied on cement samples during creep tests may accelerate the hydration rate, which in turn influences the microstructural development and the creep properties. However, it is shown from the results in Tamtsia et al. (2004) that the hydration degree profiles are very similar for the loaded and unloaded samples for both ages of loading at 24 and 30 h, and hence creep loads seem to have no effect at all on the hydration kinetics. Therefore, the hydration degree profile from the measurement for the case of loading at 24 h is used to obtain the evolution of the digital hydrating microstructures for the creep simulations of loading at both 18 and 24 h.

Simulation of Creep in Hydrating Cement Paste

The microstructures are discretized on a regular cubic mesh (element size of 1 μm) with the double burning algorithm (Do et al. 2015). The flowchart of the modeling procedure is sketched in Fig. 5. Fig. 6 shows slices of the three-dimensional digital microstructures of 100-μm size at various degrees of hydration generated from ***μic*** and the corresponding 1-μm mesh generated from the microstructures. It is important to ensure that the mesh size chosen is sufficiently fine to obtain convergence. It has been shown previously that there is little difference between the results from static and kinematic boundary conditions, implying that the simulations converge with a relatively small error at the chosen mesh size (Do et al. 2015). The effective strains developing with time of the modeled microstructure are calculated from the average strains over the CV that is under a uniaxial constant unit stress applied perpendicular to one surface and fixed zero displacement (normal direction to the surface) on the opposite surface. C-S-H is assumed to be the only source of creep in cement paste and other phases are considered to have a purely elastic response. For computational simplifications, water in saturated condition was modeled to

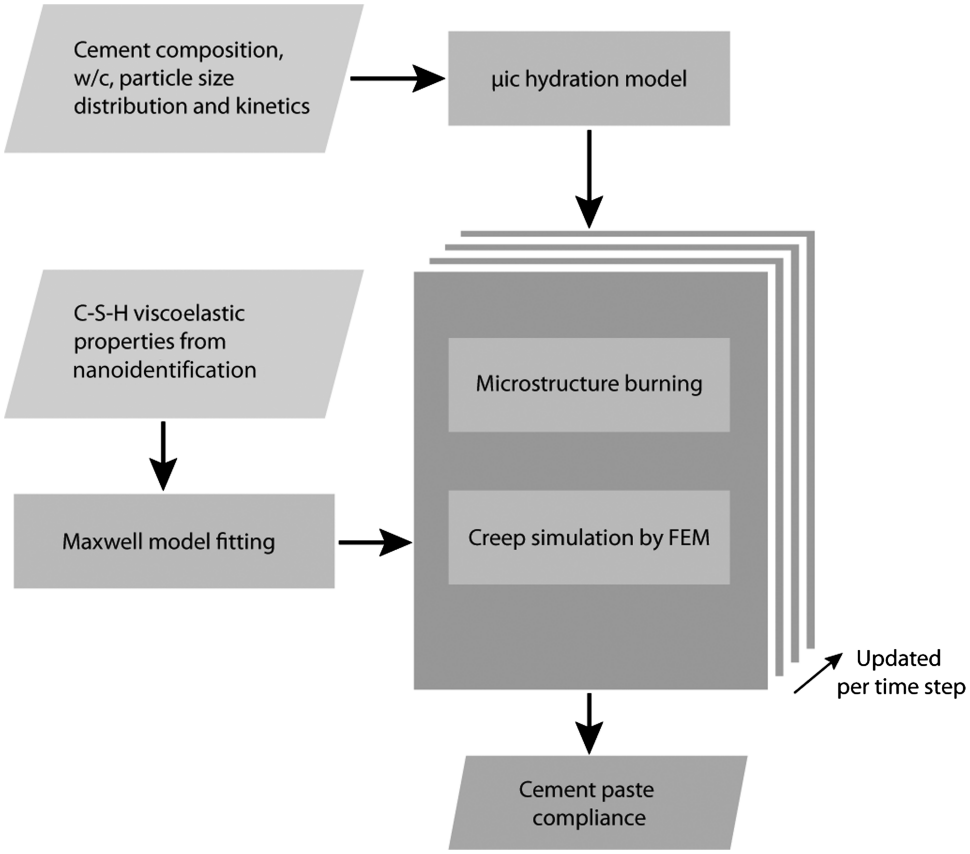

Fig. 5. Flowchart of modeling of aging creep in hardening cement paste for one given age of loading

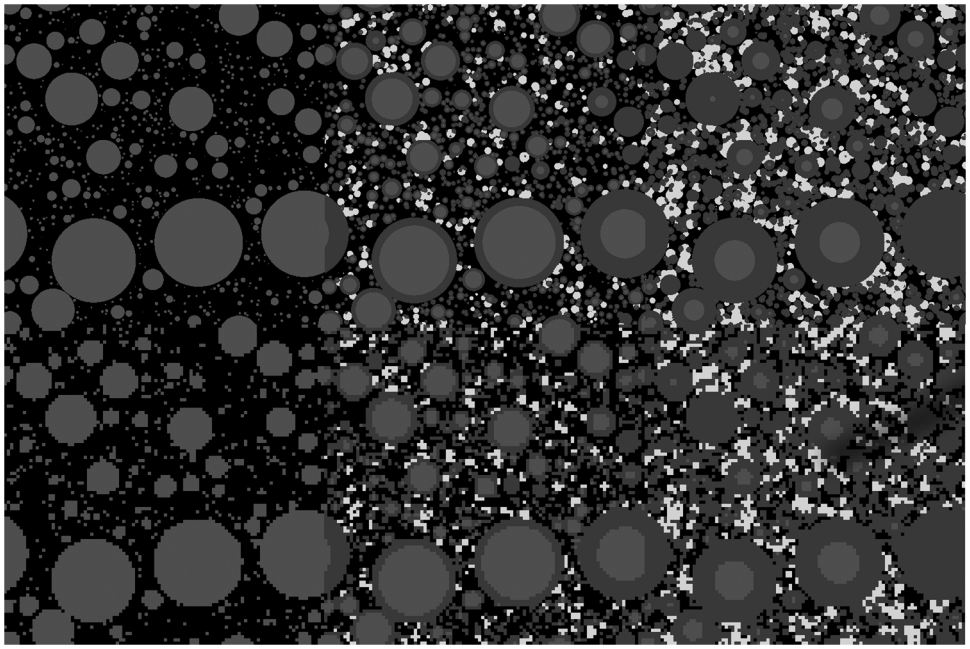

Fig. 6. Two-dimensional slices of microstructure at 0, 47, and 90% degree of hydration (top) and the corresponding mesh with 1-μm resolution (bottom); the light gray shows unhydrated cement grains, dark gray the hydration products that grow on the cement particles (e.g., C-S-H), and white the hydration products that grow in the pore-space (e.g., portlandite)

behave as a quasi-incompressible material with an extremely low elastic modulus and its flow and equalization of pore pressures were neglected. Intrinsic elastic properties of the phases and the source of the data are listed in Table 2.

The microstructural development due to continuing hydration is taken into account during the simulation of the creep process. Solidification of the load-bearing microstructure under the simulated creep is modeled by an updating procedure for new states of the microstructure, which consists of gradual filling up by newly formed hydrates including C-S-H and other elastic phases (e.g., portlandite). The total strain of the microstructure caused by the given external uniform stress (loading) applied on its boundary consists of two parts: elastic and viscous strains. The elastic part is an instantaneous deformation at the time of the externally applied loading, whereas the viscous part gradually increases with time due to the creep response of C-S-H present in the microstructure. During this viscoelastic behavior of the cement paste it is reasonable to assume that the external stress loads only hydrate elements in the initial stage (at the loading time) of the microstructure and all the newly formed hydrates after the loading time are in a free stress state regarding the applied external loading. For each simulation time step, once newly hydrated elements are formed, they take part in sustaining against the differential internal loading [i.e., the second term on the right-hand side of Eq. (52)] that is transferred due to creep in the existing C-S-H elements within each time interval. The internal loading transferring from of each C-S-H element is characterized by the logarithmic function of time whose rate is inversely proportional to time [see Eq. (55) and the viscous component shown in Fig. 2]. Due to the development of the simulated microstructure the formation of hydrates hinders the viscous deformation and thus the creep rate decreases. Although the overall average strain of the entire CV increases with time due to irrecoverable local strains [i.e., $\Delta\boldsymbol{\varepsilon}$ in Eq. (47)], the local elementary stresses are relieved [i.e., $\Delta\boldsymbol{\sigma}$ in Eq. (43)] as they are redistributed over a higher solid fraction for each time step.

The use of a constant FE mesh provides an easy updating procedure in which stress, strain states, and internal variables in the same Gaussian points can be reused without any requirement to transform the new mesh. The creep of the newly formed C-S-H elements is also easily simulated without any extra implementation effort. Each of the simulations took approximately 24 h to simulate on a single-node desktop having 12 GB of RAM.

Table 2. Intrinsic Elastic Properties of Chemical Phases Measured by Nanoindentation or Mechanical Tests

Phase	Young's modulus (GPa)	Poisson's ratio (—)	References
Water	0.001	0.499924	Šmilauer and Bažant (2010)
Alite	135	0.3	Acker (2001)
Belite	130	0.3	Velez et al. (2001)
Aluminate	145	0.3	Velez et al. (2001)
Ferrite	125	0.3	Velez et al. (2001)
Gypsum	30	0.3	Bell (1994)
C-S-H	25.55	0.24	Constantinides and Ulm (2004)
Portlandite	38	0.305	Constantinides and Ulm (2004)
Ettringite	22.4	0.25	Kamali et al. (2004)
Monosulphate	42.3	0.324	Kamali et al. (2004)
Hydrogarnet	22.4	0.25	Kamali et al. (2004)
Iron hydroxide	22.4	0.25	Kamali et al. (2004)

Note: Young's modulus of C-S-H is assumed to be the mean value from the reference.

Results and Discussion

Assuming C-S-H Constant Density $\rho = 2.0$ g/cm^3

The creep results of the hardening cement pastes for loading from 18, 24, and 30 h are shown in Fig. 7. The simulated compliances are in reasonable agreement with measured values. The relative errors

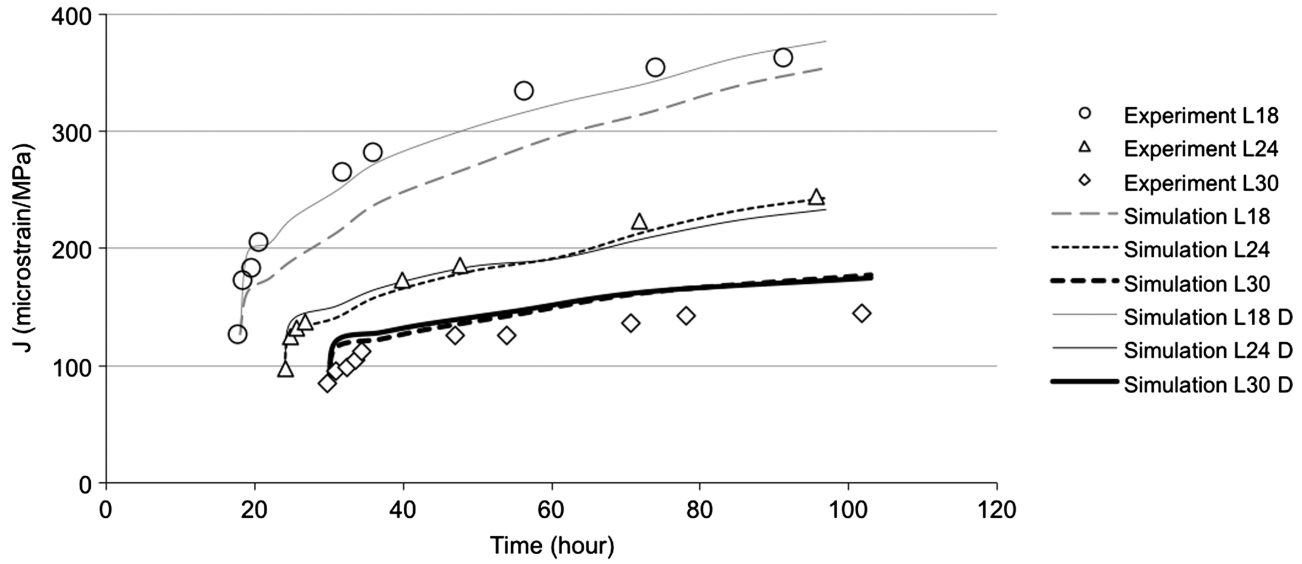

Fig. 7. Results of creep compliance in the cement pastes for three different ages of loading; L18, L24, and L30 denote loading from 18, 24, and 30 h, respectively, with constant density of C-S-H, whereas L18 D, L24 D, and L30 D denote loading from 18, 24, and 30 h, respectively, considering the effect of C-S-H densification; the experimental data reported by Tamtsia et al. (2004) were performed using the compressive stress-strength ratio of 0.3 applied to the specimens at the age of loading

of the predictions are roughly 20%, to which the experimental C-S-H fitting, FE calculation, and statistical microstructural sampling could contribute. The effect of age when loading on creep is well captured: the compliance of younger paste has a higher magnitude (of both the elastic and viscous components) due to a sparse spatial distribution of the solid phases at the early stages of hydration. It can be also seen that the simulations are able to capture the relative trends of the compliances from 24 to 30 h. However, the simulated creep is lower compared with the experimental creep for loading from 18 h. This is because the input creep function of C-S-H used in the simulation assumes a constant bulk density ρ of 2.0 g/cm^3. In fact, this value is lower at very early ages (Muller et al. 2013). The use of a higher C-S-H density leads to underestimating its creep function and consequently underestimates of the creep of the cement paste.

Assuming C-S-H Densification

The creep results of the hardening cement pastes taking into account C-S-H densification for loading from 18, 24, and 30 h are compared with ones with constant bulk C-S-H density of 2.0 g/cm^3 and to experimental values as plotted in Fig. 7. It was observed that the simulations including the effect of densification indicate a higher creep at the early ages. The agreement with the experimental results for loading at 18 h is significantly improved due to the inclusion of the effect of densification: the relative errors of the predictions are roughly 10%. Slight variations in the results are expected because the simulations with densifications did not simulate the exact same spatial arrangement of phases as was the case without densification.

To explain these observations for the two later ages of loading at 24 and 30 h, one should look back upon the calculations of elastic properties presented in Do et al. (2015). It is shown that the densification has a very little effect on the effective elastic deformation of the CV after 15% degree of hydration. This means that the densifying microstructure having a larger amount in volume of less dense C-S-H with lower intrinsic stiffness exhibits an equivalent effective elastic response comparable to the microstructure having a lesser amount in volume of the denser C-S-H with its higher intrinsic stiffness (25.55 GPa). Similarly, this equivalence on the effective viscoelastic deformations seems still to hold true for loading from 24 and 30 h: the densifying microstructure having a larger amount in volume of lower packing density C-S-H phases with their higher rates of intrinsic relaxation exhibits an equivalent effective viscoelastic behavior comparable to the microstructure having a sparer amount of denser C-S-H with its lower rate of intrinsic relaxation.

On the contrary, for loading from 18 h, the creep compliance curve of cement paste under the assumption of C-S-H densification is clearly higher than the one without it. This is an interesting result but not surprising. It is apparent in Fig. 7 that the slope of the curve with the densification is higher than the slope of the curve with the constant C-S-H density only within the range from 18 to 24 h. This implies that in this particular time range, the densification assumption suggests a higher rate of microstructural deformation. This time range coincides with the time interval when the densification process still strongly develops, and it slows down after 24 h (Fig. 3). The transient relaxation of a large amount of very low packing density C-S-H leads to the high rate of deformation from 18 to 24 h and the higher irrecoverable deformation after 24 h.

While the previous results demonstrate the strength of the techniques used, the current study is limited to a single cement at a single water-to-cement ratio. A deeper investigation is required in order to better understand the creep of C-S-H in hardening cement pastes and to obtain a more generalized method of simulating creep that would be applicable to cements of various compositions and those containing supplementary cementitious materials.

Conclusions

This paper demonstrates the strength of microstructural models in simulating the effect of the spatial distribution of cement particles and the hydration products on the development of mechanical properties of cement pastes. It was demonstrated that the complicated

processes of microstructural development and creep, which occur in parallel, could be captured and their combined effect simulated in these models.

The basic creep behavior at young ages of three-dimensional numerical microstructures of hydrating cement pastes is simulated using FEM. The generalized Maxwell model is used to numerically describe intrinsic C-S-H viscoelasticity that is obtained by nanoindentation tests. It is found that if the C-S-H phase is assumed to be homogenous with a constant bulk density ρ of 2.0 g/cm^3 (corresponding to its packing density η of 0.7) at all times, the numerical results on creep compliance of cement paste show good trends with the measured values for loading from 24 and 30 h. This model captures well the effect of age of loading that is observed in cementitious composites. However, under these assumptions the simulated creep compliance for loading from 18 h is lower than the experimental values because the input bulk density under the constant assumption is much higher than its actual value at 18 h of hydration.

If C-S-H phases are assumed to have a creep response that depends on a packing density varying with time, this densification has almost no impact on the effective deformation of the cement microstructure when loading from 24 and 30 h. However, the densifying model predicts a higher viscous deformation rate of cement paste in the period of high densification rate and thus considerably higher overall deformation of cement paste in the case of loading at 18 h. The assumption of densification of C-S-H in the simulations provides markedly better predictions of ageing creep for early-age loading on cement pastes.

Despite the robustness of the present approach particularly for early-age materials, the realistic absolute values of creep could not be predicted because relative errors of approximately 20% were obtained. In order to improve the accuracy of numerical solutions, further studies on the intrinsic creep modeling of C-S-H are necessary. Another source of weakness in the approach could arise from the necessity to discretize the microstructure into a mesh, where the size of the mesh elements may affect convergence and accuracy.

Acknowledgments

The authors gratefully acknowledge the financial support from the Swiss National Science Foundation. The authors thank Dr. A. Guidoum and Dr. M. Vandamme for fruitful discussions. The authors would also like to thank the reviewers of this article for comments that helped in significantly improving the manuscript.

References

Acker, P. (2001). "Micromechanical analysis of creep and shrinkage mechanisms." *Proc., 6th Int. Conf., CONCREEP 6 of Creep, Shrinkage and Durability Mechanics of Concrete and Other Quasi-Brittle Materials*, F. J. Ulm, Z. P. Bazant, and F. H. Wittmann, eds., Elsevier, Oxford, U.K., 15–25.

Argyris, J. H., and Kelsey, S. (1954). *Energy theorems and structural analysis*, Butterworths, London.

Bažant, Z. P. (1972). "Numerical determination of long-range stress history from strain history in concrete." *Mater. Struct.*, 5(3), 135–141.

Bažant, Z. P., and Baweja, S. (2000). "Creep and shrinkage prediction model for analysis and design of concrete structures: Model B3." *Creep and shrinkage-structural design effects, ACI SP-194*, A. Al-Manaseer, ed., American Concrete Institute, Farmington Hills, MI, 1–83.

Bell, F. (1994). "A survey of the engineering properties of some anhydrite and gypsum from the north and midlands of England." *Eng. Geol.*, 38(1-2), 1–23.

Bernard, O., Ulm, F.-J., and Germaine, J. T. (2003). "Volume and deviator creep of calcium-leached cement-based materials." *Cem. Concr. Res.*, 33(8), 1127–1136.

Bishnoi, S., and Scrivener, K. L. (2009). "Studying nucleation and growth kinetics of alite hydration using μic." *Cem. Concr. Res.*, 39(10), 849–860.

Constantinides, G., and Ulm, F. J. (2004). "The effect of two types of C-S-H on the elasticity of cement based materials: results from nanoindentation and micromechanical modelling." *Cem. Concr. Res.*, 34(1), 67–80.

Constantinides, G., and Ulm, F. J. (2007). "The nanogranular nature of C-S-H." *J. Mech. Phys. Solids.*, 55(1), 64–90.

Do, Q. H., Bishnoi, S., and Scrivener, K. L. (2013). "Numerical simulation of porosity in cements." *Transp. Porous Med.*, 99(1), 101–117.

Do, Q. H., Bishnoi, S., and Scrivener, K. L. (2015). "Microstructural modelling of the elastic properties of C3S at early ages." *Comput. Concr.*, 16(1), 125–140.

Grasley, Z. C., and Lange, D. A. (2007). "Constitutive modeling of the aging viscoelastic properties of portland cement paste." *Mech. Time-Depend. Mater.*, 11(3), 175–198.

Guidoum, A. (1994). "Simulation numérique 3D des comportenments des bétons en tant que composites granulaires [3D numerical simulation of the behavior of concrete as granular composites]." Ph.D. thesis, Ecole Polytechnique Federale de Lausanne, Lausanne, Switzerland (in French).

Huet, C. (1993). "Some basis tools and pending problems in the development of constitutive equations for the delayed behaviour of concrete." *Creep and Shrinkage of concrete*, Z. P. Bažant and I. Carol, ed., Spon, London, 189–200.

Kamali, S., Moranville, M., Garboczi, E., Prene, S., and Gerard, B. (2004). "Hydrate dissolution influence on the Young's modulus of cement pastes." *Proc., Int. Symp., Fracture Mechanics of Concrete Structures (FraMCoS-V)*, V. C. Li, et al., eds., Vail, 631–638.

Muller, A. C. A., Scrivener, K. L., Gajewicz, A. M., and McDonald, P. J. (2013a). "Densification of C-S-H Measured by 1H NMR relaxometry." *J. Phys. Chem. C*, 117(1), 403–412.

Muller, A. C. A., Scrivener, K. L., Gajewicz, A. M., and McDonald, P. J. (2013b). "Use of bench-top NMR to measure the density, composition and desorption isotherm of C-S-H in cement paste." *Microporous Mesoporous Mater.*, 178(1), 99–103.

Pichler, C., and Lackner, R. (2008). "A multiscale creep model as basic for simulation of early-age concrete behavior." *Comput. Concr.*, 5(4), 295–328.

Sanahuja, J., and Toulemonde, C. (2011). "Numerical homogenization of concrete microstructures without explicit meshes." *Cem. Concr. Res.*, 41(12), 1320–1329.

Scheiner, S., and Hellmich, C. (2009). "Continuum microviscoelasticity model for aging basic creep of early-age concrete." *J. Eng. Mech.*, 10.1061/(ASCE)0733-9399(2009)135:4(307), 307–323.

Sedef, M., Samur, E., and Basdogan, C. (2006). "Real-time finite element simulation of linear Viscoelastic tissue behavior based on experimental." *IEEE Comput. Graphics Appl.*, 26(6), 58–68.

Šmilauer, V., and Bažant, Z. P. (2010). "Identification of viscoelastic C-S-H behavior in mature cement paste by FFT-based homogenization method." *Cem. Concr. Res.*, 40(2), 197–207.

Tamtsia, B. T., Beaudoin, J. J., and Marchand, J. (2004). "The early age short-term creep of hardening cement paste load-induced hydration effects." *Cem. Concr. Res.*, 26(5), 481–489.

Taylor, H. F. W. (1997). *Cement chemistry*, Thomas Telford, London.

Thomas, J. J., Allen, A. J., and Jennings, H. M. (2009). "Hydration kinetics and microstructure development of normal and CaCl2-Accelerated tricalcium silicate pastes." *J. Phys. Chem. C*, 113(46), 19836–19844.

Thomas, J. J., and Jennings, H. M. (2006). "A colloidal interpretation of chemical aging of the C-S-H gel and its effects on the properties of cement paste." *Cem. Concr. Res.*, 36(1), 30–38.

Turner, M. J., Clough, R. W., Martin, H. C., and Topp, L. J. (1956). "Stiffness and deflection analysis of complex structure." *J. Aeronaut. Sci.*, 23(9), 805–823.

Ulm, F. J., Le Maou, F., and Boulay, C. (1999). "Creep and shrinkage coupling: New review of some evidence." *Revue Française De Génie Civil*, 3(3-4), 21–38.

Vandamme, M. (2008). "The nanogranular origin of concrete creep: A nanoindentation investigation of microstructure and fundamental properties of calcium-silicate-hydrates." Ph.D. thesis, Civil and Environmental Engineering Dept., Massachusetts Institute of Technology, Cambridge, MA.

Vandamme, M., and Ulm, F. J. (2009). "Nanogranular origin of concrete creep." *Proc. Natl. Acad. Sci.*, 106(26), 10552–10557.

Velez, K., Maximilien, S., Damido, D., Fantozzi, G., and Sorrentino, F. (2001). "Determination by nanoindentation of elastic modulus and hardness of pure constituents of Portland cement clinker." *Cem. Concr. Res.*, 31(4), 555–561.

Wendner, R., Hubler, M. H., and Bažant, Z. P. (2015). "Statistical justification of model B4 for multi-decade concrete creep using laboratory and bridge databases and comparisons to other models." *Mater. Struct.*, 48(4), 815–833.

Zienkiewicz, O. C., and Taylor, R. L. (2000). *The finite element method, Solid mechanics*, 5th Ed., Vol. 2, Butterworth-Heinemann, Oxford, U.K.

Zienkiewicz, O. C., Watson, M., and King, I. P. (1968). "A numerical method of visco-elastic stress analysis." *Int. J. Mech. Sci.*, 10(10), 807–827.

Erratum for "Microstructural Modeling of Early-Age Creep in Hydrating Cement Paste" by Quang Huy Do, Shashank Bishnoi, and Karen L. Scrivener

Quang Huy Do

Postdoctoral Researcher, Faculty of Mechanical, Maritime and Materials Engineering, Dept. of Marine and Transportation Technology, Delft Univ. of Technology, 2628 CD, Delft, Netherlands. E-mail: huy78.do@gmail.com

Shashank Bishnoi

Assistant Professor, Dept. of Civil Engineering, Indian Institute of Technology Delhi, New Delhi 110016, India (corresponding author). E-mail: bishnoi@iitd.ac.in

Karen L. Scrivener

Professor, Laboratory of Construction Materials, Ecole Polytechnique Fédérale de Lausanne, EPFL-STI-IMX-LMC, Station 12, 1015 Lausanne, Switzerland. E-mail: karen.scrivener@epfl.ch

Some of the references cited in the original paper do not best represent the work used as background for its work. The authors do not, in any way, take credit for the solidification model (Bažant 1977; Bažant and Prasannan 1988) and exponential algorithm for aging creep (Bažant 1982; Bažant and Wu 1974) referred to in the original paper. The main intent of the original paper is to present the implementation of creep on a microstructural model and to show the importance of considering the increasing density of the C–S–H phase. The authors regret any misunderstanding that may have arisen due to the inadvertent omission of these references, which, it is now understood, are more suitable for the current work.

References

Bažant, Z. P. (1982). "Mathematical models for creep and shrinkage of concrete." Chapter 7, *Creep and shrinkage in concrete structures*, Z. P. Bažant and F. H. Wittmann, eds., Wiley, London, 163–256.

Bažant, Z. P. (1977). "Viscoelasticity of solidifying porous material—Concrete." *J. Eng. Mech. Div.*, 103(6), 1049–1067.

Bažant, Z. P., and Prasannan, S. (1988). "Solidification theory for aging creep." *Cem. Concr. Res.*, 18(6), 923–932.

Bažant, Z. P., and Wu, S. T. (1974). "Creep and shrinkage law of concrete at variable humidity." *J. Eng. Mech. Div.*, 100(6), 1183–1209.